

Nobeyama 45m Cygnus-X CO survey I: photodissociation of molecules revealed by the unbiased large-scale CN and C¹⁸O maps

M. Yamagishi¹, A. Nishimura², S. Fujita², T. Takekoshi³, M. Matsuo⁴, T. Minamidani^{4,5}, K. Taniguchi^{4,5}, K. Tokuda^{6,7}, Y. Shimajiri⁸

yamagish@ir.isas.jaxa.jp

ABSTRACT

We present an unbiased large-scale (9 deg²) CN ($N=1-0$) and C¹⁸O ($J=1-0$) survey of Cygnus-X conducted with the Nobeyama 45m Cygnus-X CO survey. CN and C¹⁸O are detected in various objects towards the Cygnus-X North and South (e.g., DR17, DR18, DR21, DR22, DR23, and W75N). We find that CN/C¹⁸O integrated intensity ratios are systematically different from region to region, and are especially enhanced in DR17 and DR18 which are irradiated by the nearby OB stars. This result suggests that CN/C¹⁸O ratios are enhanced via photodissociation reactions. We investigate the relation between the CN/C¹⁸O ratio and strength of the UV radiation field. As a result, we find that CN/C¹⁸O ratios correlate with the far-UV intensities, G_0 . We also find that CN/C¹⁸O ratios decrease inside molecular clouds, where the interstellar UV radiation is reduced due to the interstellar dust extinction. We conclude that the CN/C¹⁸O ratio is controlled by the UV radiation, and is a good probe of photon-dominated regions.

Subject headings: submillimeter: ISM, ISM: photon-dominated region (PDR), molecules, individual object (Cygnus-X)

¹Institute of Space and Astronautical Science, Japan Aerospace Exploration Agency, Chuo-ku, Sagami-hara 252-5210, Japan

²Graduate School of Science, Nagoya University, Furo-cho, Chikusa-ku, Nagoya 464-8602, Japan

³Institute of Astronomy, The University of Tokyo, 2-21-1 Osawa, Mitaka, Tokyo 181-0015, Japan

⁴Nobeyama Radio Observatory, National Astronomical Observatory of Japan (NAOJ), National Institutes of Natural Sciences (NINS), 462-2, Nobeyama, Minamimaki, Minamisaku, Nagano 384-1305, Japan

⁵Department of Astronomical Science, School of Physical Science, SOKENDAI (The Graduate University for Advanced Studies), 2-21-1, Osawa, Mitaka, Tokyo 181-8588, Japan

⁶National Astronomical Observatory of Japan, National Institutes of Natural Sciences, 2-21-1 Osawa, Mitaka, Tokyo 181-8588, Japan

⁷Graduate School of Science, Osaka Prefecture University, 1-1 Gakuen-cho, Naka-ku, Sakai, Osaka 599-8531, Japan

⁸Laboratoire AIM, CEA/DSM-CNRS-Université Paris Diderot, IRFU/Service d'Astrophysique, CEA Saclay, F-91191 Gif-sur-Yvette, France

1. Introduction

A deep understanding of the interactions between the ultraviolet (UV) radiation and the interstellar medium (ISM) is essential to study evolutions of molecules in the Universe. The most common sites for such interactions are PDRs (photon dominated regions), where photodissociation and photoionization reactions are the most relevant processes. One of the most commonly used probes of PDRs in radio astronomy is CN (Fuente et al. 1993; Greaves & Church 1996; Simon et al. 1997; Fuente et al. 2005); one of the formation pathways leading to CN is photodissociation of HCN. Based on their models, Boger & Sternberg (2005) showed that CN/HCN abundance ratios are high at the surface of a molecular cloud due to significant contribution of the interstellar UV radiation. Another important probe is a rare isotope of CO (Glassgold et al. 1985; Yurimoto & Kuramoto 2004); UV radiation selectively dissociates rare CO isotopes more effectively than major CO isotopes because of the difference in the self shielding (Lada et al. 1994; Shimajiri et al. 2014; Lin et al. 2016). Until now, however, studies of PDR probes are still limited, and there is no consensus about what the most reliable PDR probe is, because mapping observations of such weak lines are difficult even for high-mass star-forming regions. Hence it is valuable to test possible PDR probes for a variety of high-mass star-forming regions.

Among many Galactic high-mass star-forming regions, Cygnus-X ($d=1.4$ kpc; Rygl et al. 2012) is one of the best sites to study interactions between UV and the ISM. Cygnus-X consists of nine OB associations (Humphreys 1978). The most active and well-known one is Cygnus OB2 association which includes 169 OB stars (Wright et al. 2015). Cygnus-X is roughly divided into two regions: the Cygnus-X North and South. Cygnus-X North shows many filamentary structures in infrared and radio. Many young stellar objects (YSOs) are associated with Cygnus-X North (Beerer et al. 2010). By contrast, Cygnus-X South shows relatively diffuse structures, and the star-formation activity is less intense; Schneider et al. (2006) showed that the average density and excitation temperature of CO in Cygnus-X North are higher than those in Cygnus-X South, and suggested that Cygnus-X North is a more active star-forming region. Cygnus-X has been intensively observed in many studies, which are summarized by Reipurth & Schneider (2008). In addition, recent large-area surveys of Cygnus-X have been performed by James Clerk Maxwell Telescope (JCMT; Gottschalk et al. 2012), Five College Radio Astronomical Observatory (FCRAO; Schneider et al. 2011), *Spitzer* (Hora et al. 2007), *Herschel* (Schneider et al. 2016), and the Balloon-borne Large Aperture Submillimeter Telescope (BLAST; Roy et al. 2011).

In this paper, we present unbiased large-scale CN ($N=1-0$) and $C^{18}O$ ($J=1-0$) maps of Cygnus-X, and test the availability of the CN/ $C^{18}O$ integrated intensity ratio as a PDR probe. Since CN will be enhanced and $C^{18}O$ will be selectively dissociated in PDRs, CN/ $C^{18}O$ ratios are expected to be sensitive to the UV radiation. The present study is based on the Nobeyama 45m Cygnus-X CO survey (PI: A. Nishimura), where ^{12}CO ($J=1-0$), ^{13}CO ($J=1-0$), $C^{18}O$ ($J=1-0$), and CN ($N=1-0$) were simultaneously observed for a 9 deg^2 area thanks to the large-scale mapping capability and the wide frequency coverage of the facility. The simultaneous observations ensure reliability of the resultant CN and $C^{18}O$ data. The number of unbiased CO multi-line surveys for high-

mass star-forming regions with high angular resolution is still limited (Orion: Nishimura et al. 2015; Shimajiri et al. 2014, Galactic plane: Barnes et al. 2015; Umemoto et al. 2017). As for CN, such survey is even more limited (Rodriguez-Franco et al. 1998; Barnes et al. 2015; Pety et al. 2017). Therefore, our survey will provide a valuable data set not only for PDR studies but also for comparison to other surveys of Cygnus-X and for a general understanding of the ISM in massive star forming regions. In this paper, we use the C^{18}O data for comparison to the CN data. In addition, we supplementarily use the ^{13}CO data for analyses of the CN and C^{18}O data. Detailed analyses of the C^{18}O and ^{13}CO data (e.g., properties of dense cores) will be presented in separate papers.

2. Observation and data reduction

The observations of Cygnus-X were carried out during 2016 January 13 and May 08 with the Nobeyama 45m/FOREST+SAM45. The total observation time was 77 hrs. The four-beam receiver FOREST (Minamidani et al. 2016) allows simultaneous multi-line on-the-fly mapping. In the present survey, ^{12}CO ($J=1-0$; 115.271202 GHz), ^{13}CO ($J=1-0$; 110.201354 GHz), C^{18}O ($J=1-0$; 109.782176 GHz), and CN ($N=1-0$, $J=3/2-1/2$, $F=5/2-3/2$; 113.490982 GHz) were simultaneously observed in the single polarization mode. The survey area is shown in Fig. 1, which covers both the Cygnus-X North and South as well as the Cygnus OB2 association. The overall observed area is 9 deg^2 , which was covered by mosaic sub-maps with $1^\circ \times 1^\circ$. The OTF scan parameters are the same as the FUGIN galactic plane survey (Umemoto et al. 2017); the RX angle, scan spacing, scan length, scan speed, and sampling time are $9.''46$, $8.''5$, $3600''$, $100''/\text{sec}$, and 40 msec, respectively. The typical system temperatures including atmosphere are 350 K, 200 K, 150 K, and 150 K for ^{12}CO , CN, ^{13}CO , and C^{18}O , respectively. We performed multiple scans to achieve Nyquist sampling for each sub-map. Pointing errors were corrected every 1.5 hr by observing a SiO maser source, AU Cyg. As a result, the pointing accuracy of the telescope was kept to be $< 5''$.

Data reduction was performed by using the NOSTAR software provided by the Nobeyama Radio Observatory. For each map, we split data to each array, and subtracted baselines using a first-order polynomial. The velocity ranges to subtract baselines are $-150 - -90$ and $30 - 100 \text{ km s}^{-1}$ for CN, $-150 - -20$ and $20 - 100 \text{ km s}^{-1}$ for C^{18}O , and $-150 - -60$ and $25 - 100 \text{ km s}^{-1}$ for ^{13}CO . The amplitude of line intensities was calibrated based on the observational results of W51 and DR21. The calibration method is the same as that applied in the FUGIN project (Umemoto et al. 2017). We used a spatial grid of $22.''7$ and a velocity grid of 0.5 km s^{-1} to obtain high signal-to-noise ratio maps. Bessel-Gauss function was used for the convolution. The effective angular resolution is $46''$ (0.30 pc at $d=1.4 \text{ kpc}$). The typical noise levels of the final CN, C^{18}O , and ^{13}CO data are 0.38 K, 0.26 K, and 0.27 K, respectively, in T_{mb} scale. The final calibrated FITS cube of CN will

be publicly released on the web¹². We also plan to release the FITS cubes of ^{12}CO , ^{13}CO , and C^{18}O after publishing the forthcoming science papers.

3. Results

Figure 2 shows examples of the CN, C^{18}O , and ^{13}CO spectra extracted from local peaks in DR21, DR18, and DR17, where the CN intensities are the strongest in the observed area. The intensity ratios of C^{18}O to ^{13}CO are $\sim 1/6$ in the local peaks. Line ratios of CN to C^{18}O and the CN hyperfine lines are different from region to region, suggesting that optical depths and/or excitation states are different among the regions. The theoretical CN hyperfine line intensities relative to that of the strongest line are 0.37, 0.30, and 0.30 for $F=3/2-1/2$, $F=1/2-1/2$, and $F=3/2-3/2$ transitions, respectively, assuming the local thermodynamic equilibrium and the optically thin limit (Skatrud et al. 1983). Among the regions, hyperfine line ratios in DR21 are larger than the theoretical values (0.57 ± 0.05 , 0.42 ± 0.04 , and 0.44 ± 0.04 for $F=3/2-1/2$, $F=1/2-1/2$, and $F=3/2-3/2$ transitions, respectively), while those in DR17 and DR18 are roughly comparable to the theoretical values. Therefore, CN may be optically thick in the local peak of DR21. Unfortunately, the noise level of the CN data is too large to discuss the hyperfine line ratios except for strong local peaks. The fraction of regions where the CN hyperfine line ratio has $S/N > 3$ is only $\sim 10\%$ of the whole region. Therefore, we use only the strongest CN line in the following discussion, and do not discuss variations of hyperfine line ratios and optical depth derived from the ratios.

Figure 3 shows integrated intensity maps of CN and C^{18}O , where emission in a range of $\pm 3 \text{ km s}^{-1}$ relative to the systemic velocity is integrated. Systemic velocity in each position is determined from the peak of the corresponding ^{13}CO spectrum obtained in the present survey because ^{13}CO , C^{18}O , and CN have the mostly same velocity (Fig. 2). Many spatial structures are clearly recognized in the maps. It should be noted that the spatial extent of the CN and C^{18}O maps is comparable. The critical density of C^{18}O is $\sim 10^3 \text{ cm}^{-3}$ (Schöier et al. 2005), which is consistent with those estimated from observations (Ikeda & Kitamura 2009). In addition, the effective critical density of CN is $\sim 10^{3-4} \text{ cm}^{-3}$ (Shirley 2015). Therefore, the similarity on the spatial extent suggests that both CN and C^{18}O are emitted from regions with the density of $\sim 10^{3-4} \text{ cm}^{-3}$. Notice that C^{18}O is widely distributed in both the North and South, while CN is rather concentrated in the North. The spatial distribution of C^{18}O indicates that dense molecular gas is widely present in the North and South. A remarkable difference between the North and South is the star-formation activity; the North shows more active star formation than the South (Schneider et al. 2006). These results suggest that the CN abundance is not simply proportional to the column density of molecular gas, and is related to the star-formation activity.

¹ <https://cygnus45.github.io/>

² <http://www.nro.nao.ac.jp/~nro45mrt/html/results/data.html>

Figure 4 shows correlation between the CN and C¹⁸O integrated intensities, where there is a significant correlation as a whole ($R=+0.65$, $N=2057$). There is, however, a large variation in the CN/C¹⁸O integrated intensity ratios. In order to identify the origin of the large variation, data points in the three CN intense regions (DR21, DR18, and DR17) are color coded. It is clear that CN/C¹⁸O ratios are systematically different among the CN intense regions, and that CN/C¹⁸O ratios are especially enhanced in DR18 and DR17. Additionally, CN/C¹⁸O ratios are not likely to be uniform even within a region; CN/C¹⁸O ratios significantly vary, ranging from 0.5 to 3 for DR21, from 2 to 3 for DR18, and from 1 to 5 for DR17. In order to show significance of the variations, we fit a linear function to the data in Fig. 4, and obtain reduced chi-square of 5.0, 0.64, 2.2 for DR21, DR18, and DR17, respectively, which indicates that CN/C¹⁸O ratios are not uniform in DR21 and DR17 with the 99% confidence level. These results suggest that CN/C¹⁸O ratios are strongly affected by the differences in the local interstellar environment.

The position showing intense CN emission in DR17 corresponds to one of the DR17 pillars identified by Schneider et al. (2006) using KOSMA ¹³CO (2–1) data. They suggested that the pillar structures are locally shaped by OB stars in DR17. Gottschalk et al. (2012) also identified the same structure using JCMT ¹²CO (3–2) data, and showed that the cometary structure points to the stellar cluster Cl 14, which contains 12 OB stars. In addition, Schneider et al. (2006) detected a molecular clump in DR18. They argued that the clump is affected by the Cygnus OB2 cluster since it has an illuminated tip facing the cluster and a tail pointing away from its center. Comerón & Torra (1999) found that the molecular clump in DR18 is also illuminated by a nearby B0.5V type star. As already discussed in these studies, DR17 and DR18 have cometary structures which are likely to be formed by the intense UV radiation from the nearby OB stars. Hence the enhancement of CN/C¹⁸O ratios may be caused by the difference in the UV radiation environment. A part of DR21 also shows high CN/C¹⁸O ratios comparable with DR17 and DR18, although DR21 does not show such clear cometary structures. Considering a number of widely distributed massive stars and YSOs around DR21 (Beer et al. 2010), it is possible that intense interstellar UV radiation due to nearby massive stars enhances the CN/C¹⁸O ratios. Alternatively, deeply embedded massive stars may locally enhance the CN/C¹⁸O ratios from inside the molecular cloud.

4. Discussion

Connection between the CN/C¹⁸O ratio and the UV radiation is suggested in the previous section. We quantify the strength of the UV radiation, and directly examine the relation between the CN/C¹⁸O ratio and the UV radiation. As a probe of the UV radiation, we use the far-UV intensity normalized to that of the solar neighborhood, G_0 , which is estimated using dust temperature (T_{dust}): $G_0 = (T_{\text{dust}}/12.2 \text{ K})^5$ (Hollenbach et al. 1991). Hollenbach et al. (1991) assumed the typical density in PDRs of 10^{2-5} cm^{-3} . As discussed in the previous section, both C¹⁸O and CN are likely to be originated from regions with $\sim 10^{3-4} \text{ cm}^{-3}$, which is comparable with the typical density. Therefore, the equation is applicable throughout the observed area. The dust temperature

was derived from the color of the *Herschel*/PACS 70 μm and 160 μm maps which were retrieved from NASA/IPAC Infrared Science Archives, assuming the power-law dust emissivity index of $\beta = 1$. The background emission was estimated from a region ($l=80.88^\circ$, $b=2.47^\circ$), and subtracted from the maps. The 70 μm and 160 μm bands are suitable for deriving temperature of the warm dust component heated by the UV radiation. Since warm dust shows small β (e.g., Rodón et al. 2010), we assumed $\beta=1$. The temperature estimated in Schneider et al. (2016) is lower than that in the present study by 10–15 K, which is caused by differences in the photometric bands and β (160–500 μm maps; $\beta=2$). Figure 5 shows the CN/C¹⁸O ratios plotted against G_0 . We find that CN/C¹⁸O ratios significantly correlate with G_0 ($R=+0.997$, $N=5$) in $G_0 < 150$, indicating that the CN/C¹⁸O ratios are enhanced by the intense UV radiation via photodissociation reactions. This result also indicates that the CN/C¹⁸O ratio is a good probe of PDRs. In regions with $G_0 > 150$, CN/C¹⁸O ratios are not likely to follow the relation determined in $G_0 < 150$. One possible cause of the discrepancy is the overestimate of G_0 ; since one-component modified blackbody is assumed to estimate T_{dust} , G_0 is overestimated if emission from even warmer component and/or stochastic heating contaminates the 70 μm map. Another possibility is the underestimate of CN/C¹⁸O ratios; CN might be photo-dissociated due to the UV radiation (Boger & Sternberg 2005).

Next, we examine variations of CN/C¹⁸O ratios inside molecular clouds. Figure 6 shows CN/C¹⁸O ratios as a function of C¹⁸O integrated intensities, which roughly correspond to A_V . As seen in the figure, there is a declining trend between CN/C¹⁸O ratios and C¹⁸O integrated intensities. Note that there are no data points in the lower left corner due to an observational bias (i.e., detection limit of CN). We, however, argue that the declining trend is real because there are also no data points in the upper right corner. The overall declining trend in Fig. 6 is interpreted as a simple situation: a molecular cloud illuminated by the interstellar (external) UV radiation from the nearby massive stars. In this situation, photodissociation reactions are expected to be active at the surface of a molecular cloud (i.e., small C¹⁸O integrated intensity), while they are not inside a molecular cloud (i.e., large C¹⁸O integrated intensity) because the UV radiation is reduced due to the interstellar extinction. Therefore, the regions with high and low CN/C¹⁸O ratios may correspond to the surface and inside of the molecular clouds, respectively. In order to support this idea, the data points in Fig. 6 are color-coded according to the dust temperature because the dust temperature is also available as a probe of the position in a cloud; dust temperature decrease from the surface to inside of a molecular cloud in the simple situation. The median of CN/C¹⁸O ratios are 0.81, 1.03, 1.34, and 1.41 for regions with $T_{\text{dust}} < 26$ K, $26 \text{ K} < T_{\text{dust}} < 29$ K, $29 \text{ K} < T_{\text{dust}} < 32$ K, and $T_{\text{dust}} > 32$ K, respectively. The CN/C¹⁸O ratio increases with the dust temperature, which is also consistent with the simple situation. Hence the variations in the CN/C¹⁸O ratio as a function of the C¹⁸O integrated intensity and the dust temperature suggest that CN/C¹⁸O ratios are high at surfaces of molecular clouds illuminated by the interstellar UV radiation, while they are low inside molecular clouds due to the weak UV radiation.

We finally check variations of CN/C¹⁸O ratios on the local map. Since most of the CN and C¹⁸O detected regions are too small to examine the inner structures with the beam in the present

study (46''), we focus on the DR21 region which is the largest region where CN and C¹⁸O are detected (Fig. 3). Figure 7 shows the CN/C¹⁸O ratio map of DR21. In the map, CN/C¹⁸O ratios are high in the outer part of the molecular cloud, while they are low inside the cloud; the median of CN/C¹⁸O ratios at the outer (C¹⁸O integrated intensity <5 K km s⁻¹; 2nd contour in Fig. 7) and inner (>5 K km s⁻¹) parts are 1.90 and 1.15, respectively. This variation is consistent with Fig. 6, and supports that photodissociation reactions due to the interstellar UV radiation is dominant at the outer part of DR21. In addition, we find that CN/C¹⁸O ratios are locally enhanced near the star-forming sites (DR21 and DR21(OH)), suggesting that contribution of UV emission from embedded massive stars is not negligible. However, since CN/C¹⁸O ratios at the positions of DR21 and DR21(OH) (~1.2) are smaller than that at the surface (1.90), the UV emission from embedded massive stars may not be the dominant factor to affect CN/C¹⁸O ratios in DR21. These map-based results confirm that variations of CN/C¹⁸O ratios are consistent with the characteristics of the interaction between the ISM and UV. Hence we conclude that the CN/C¹⁸O ratio is controlled by the UV radiation, and is available as a good probe of PDRs.

5. Conclusion

We have tested the availability of the CN/C¹⁸O ratio as a PDR probe for Cygnus-X based on unbiased large scale (9 deg²) CN and C¹⁸O maps obtained in the Nobeyama 45m Cygnus-X CO survey. CN and C¹⁸O are detected in a variety of objects in the Cygnus-X North and South. C¹⁸O is widely distributed in both the Cygnus-X North and South, while CN is rather concentrated in the North, suggesting that the star formation activity is related to the CN formation. We find that there is a significant correlation between CN and C¹⁸O integrated intensities, although there is a large variation in CN/C¹⁸O ratios. We also find that the CN/C¹⁸O ratios are systematically different from region to region, and they are especially enhanced in DR17 and DR18 which are irradiated by the nearby OB stars. This result suggests that CN/C¹⁸O ratios are enhanced by the intense UV radiation via photodissociation reactions. Based on the results, we investigate the relation between the CN/C¹⁸O ratio and strength of the UV radiation, and find that CN/C¹⁸O ratios positively correlate with G_0 . We also find that CN/C¹⁸O ratios tend to decrease inside molecular clouds, where the interstellar UV radiation is reduced due to the interstellar extinction. Variations of CN/C¹⁸O ratios are consistent with the characteristics of the interaction between the ISM and UV. Hence we conclude that the CN/C¹⁸O ratio is controlled by the UV radiation, and is available as a good probe of PDRs.

We express many thanks to the anonymous referee for useful comments. This work is based on observations with the 45m telescope in the Nobeyama Radio Observatory (NRO). NRO is a branch of the National Astronomical Observatory of Japan, National Institutes of Natural Sciences. This work is also based on archival data obtained with the Herschel Space Observatory (Observation IDs: 1342244168, 1342257386, 1342196917, 1342244170, 1342211307, 1342257384). Data analysis

was carried out on the open use data analysis computer system at the Astronomy Data Center, ADC, of the National Astronomical Observatory of Japan. This research is supported by JSPS KAKENHI Grant Number JP17842380.

REFERENCES

- Barnes, P. J., Muller, E., Indermuehle, B., et al. 2015, *ApJ*, 812, 6
- Beerer, I. M., Koenig, X. P., Hora, J. L., et al. 2010, *ApJ*, 720, 679
- Boger, G. I., & Sternberg, A. 2005, *ApJ*, 632, 302
- Comerón, F., & Torra, J. 1999, *A&A*, 349, 605
- Fuente, A., García-Burillo, S., Gerin, M., et al. 2005, *ApJ*, 619, L155
- Fuente, A., Martín-Pintado, J., Cernicharo, J., & Bachiller, R. 1993, *A&A*, 276, 473
- Glassgold, A. E., Huggins, P. J., & Langer, W. D. 1985, *ApJ*, 290, 615
- Gottschalk, M., Kothes, R., Matthews, H. E., Landecker, T. L., & Dent, W. R. F. 2012, *A&A*, 541, A79
- Greaves, J. S., & Church, S. E. 1996, *MNRAS*, 283, 1179
- Hollenbach, D. J., Takahashi, T., & Tielens, A. G. G. M. 1991, *ApJ*, 377, 192
- Hora, J., Adams, J., Allen, L., et al. 2007, *Spitzer Proposal*
- Humphreys, R. M. 1978, *ApJS*, 38, 309
- Ikeda, N., & Kitamura, Y. 2009, *ApJ*, 705, L95
- Lada, C. J., Lada, E. A., Clemens, D. P., & Bally, J. 1994, *ApJ*, 429, 694
- Lin, S.-J., Shimajiri, Y., Hara, C., et al. 2016, *ApJ*, 826, 193
- Minamidani, T., Umemoto, T., Nishimura, A., et al. 2016, in *EAS Publications Series*, Vol. 75, *EAS Publications Series*, 193–194
- Nishimura, A., Tokuda, K., Kimura, K., et al. 2015, *ApJS*, 216, 18
- Pety, J., Guzmán, V. V., Orkisz, J. H., et al. 2017, *A&A*, 599, A98
- Reipurth, B., & Schneider, N. 2008, *Star Formation and Young Clusters in Cygnus*, ed. B. Reipurth, 36
- Rodón, J. A., Zavagno, A., Baluteau, J.-P., et al. 2010, *A&A*, 518, L80

- Rodriguez-Franco, A., Martin-Pintado, J., & Fuente, A. 1998, *A&A*, 329, 1097
- Roy, A., Ade, P. A. R., Bock, J. J., et al. 2011, *ApJ*, 727, 114
- Rygl, K. L. J., Brunthaler, A., Sanna, A., et al. 2012, *A&A*, 539, A79
- Schneider, N., Bontemps, S., Simon, R., et al. 2006, *A&A*, 458, 855
- . 2011, *A&A*, 529, A1
- Schneider, N., Bontemps, S., Motte, F., et al. 2016, *A&A*, 591, A40
- Schöier, F. L., van der Tak, F. F. S., van Dishoeck, E. F., & Black, J. H. 2005, *A&A*, 432, 369
- Shimajiri, Y., Kitamura, Y., Saito, M., et al. 2014, *A&A*, 564, A68
- Shirley, Y. L. 2015, *PASP*, 127, 299
- Simon, R., Stutzki, J., Sternberg, A., & Winnewisser, G. 1997, *A&A*, 327, L9
- Skatrud, D. D., De Lucia, F. C., Blake, G. A., & Sastry, K. V. L. N. 1983, *Journal of Molecular Spectroscopy*, 99, 35
- Umemoto, T., Minamidani, T., Kuno, N., et al. 2017, *PASJ*, 69, 78
- Wright, N. J., Drew, J. E., & Mohr-Smith, M. 2015, *MNRAS*, 449, 741
- Yurimoto, H., & Kuramoto, K. 2004, *Science*, 305, 1763

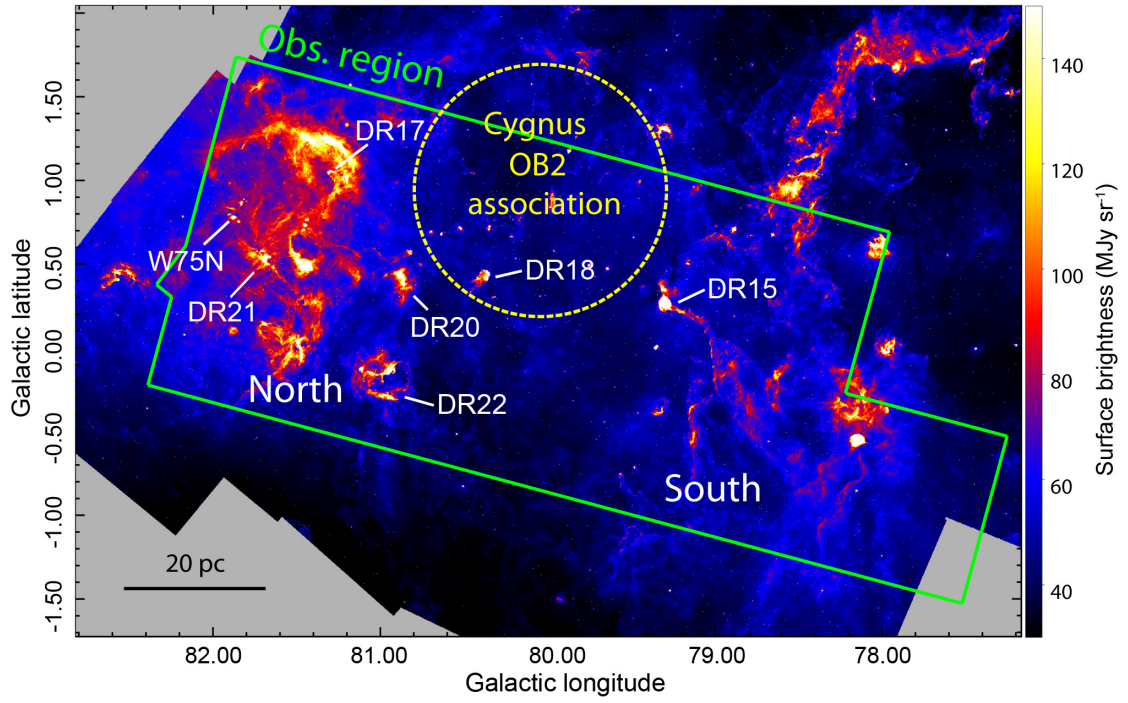


Fig. 1.— Survey area overlaid on the *Spitzer*/IRAC 8 μ m map taken by the *Spitzer* Cygnus-X legacy survey (Hora et al. 2007).

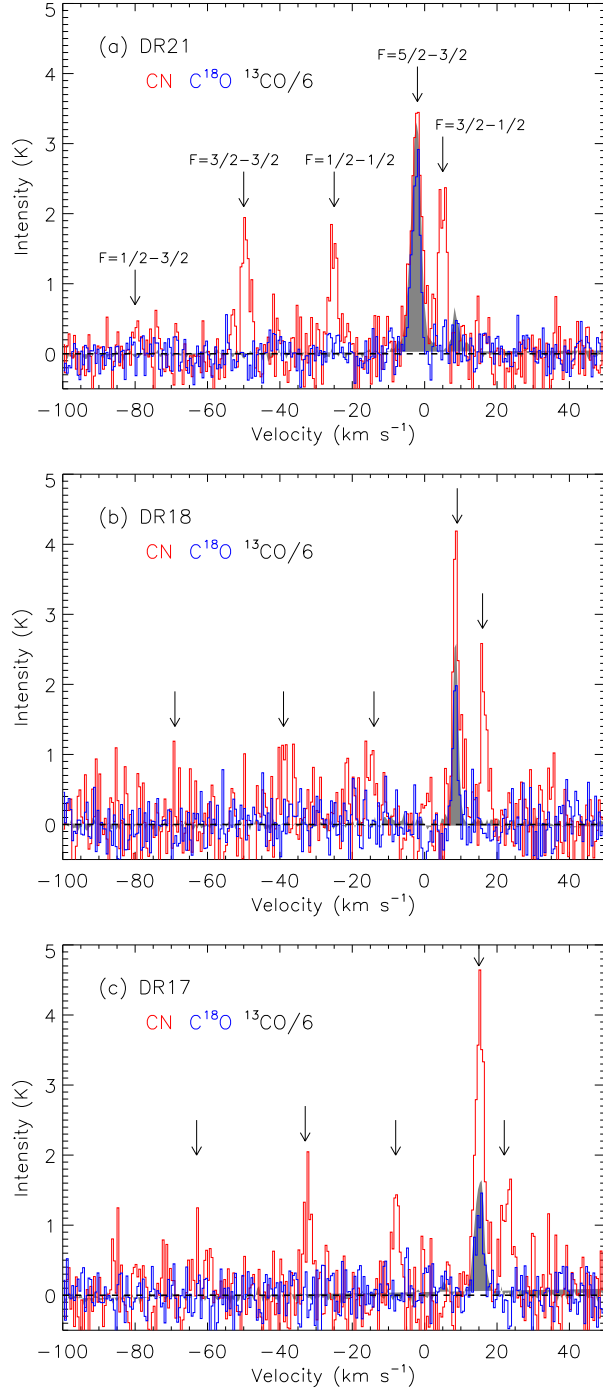


Fig. 2.— Examples of CN (red), C¹⁸O (blue), and ¹³CO (gray shade) spectra extracted from local peaks in (a) DR21 ($l=81.681^\circ$, $b=0.546^\circ$), (b) DR18 ($l=80.369^\circ$, $b=0.451^\circ$), and (c) DR17 ($l=81.302^\circ$, $b=1.050^\circ$). Downward arrows indicate velocities of the five CN hyperfine lines.

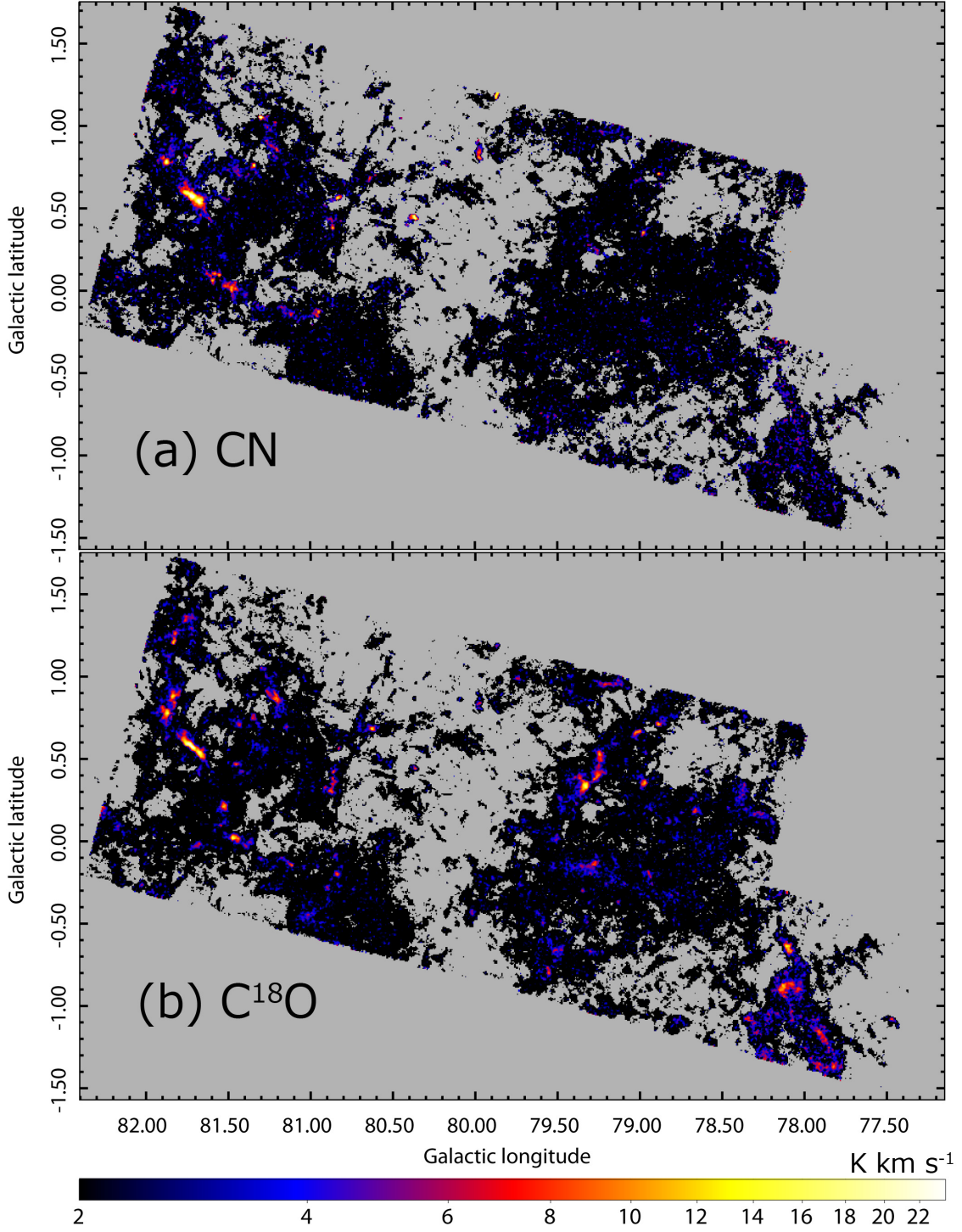


Fig. 3.— Integrated intensity maps of (a) CN ($N=1-0$, $J=3/2-1/2$, $F=5/2-3/2$) and (b) C^{18}O ($J=1-0$). Regions where ^{13}CO emission is not significantly detected are masked out.

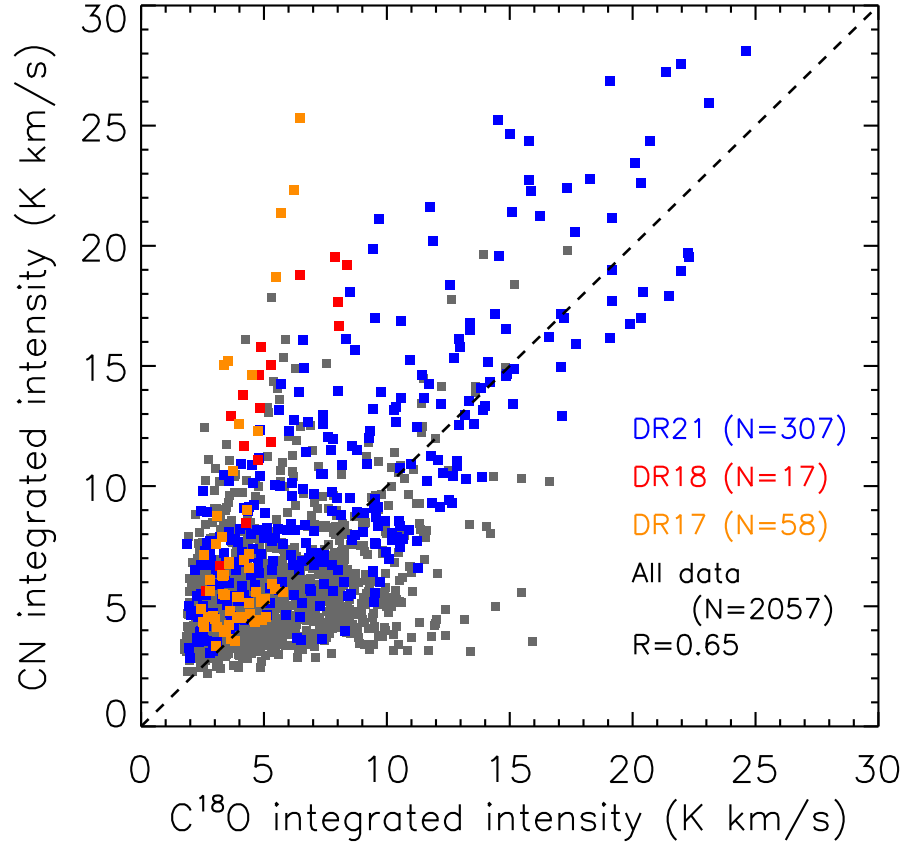


Fig. 4.— Correlation between the integrated intensities of CN and C^{18}O . Regions where both CN and C^{18}O are significantly detected ($S/N > 3$) are plotted. Linear correlation coefficient for all the data and the number of data points are shown in the bottom right.

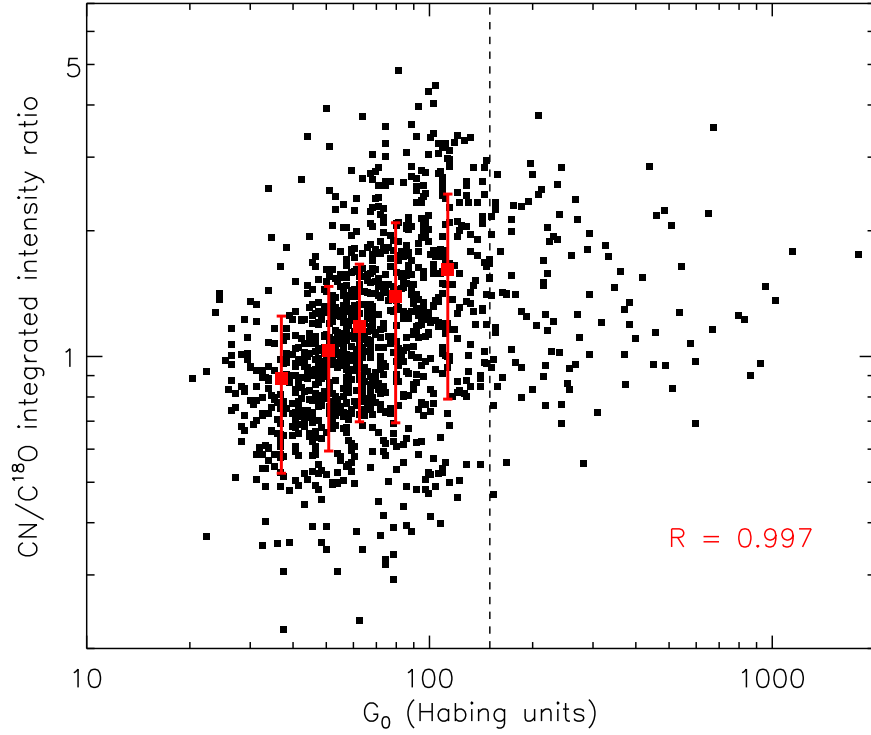


Fig. 5.— CN/C¹⁸O integrated intensity ratios plotted against G_0 for regions where CN/C¹⁸O ratios are detected with $S/N > 3$. The red data points show averages calculated for five G_0 ranges in $G_0 < 150$ (dashed line), where each G_0 range includes ~ 220 data points. The red errorbar indicates 1σ standard deviation in each G_0 range. The correlation coefficient for the red data is shown in the bottom right.

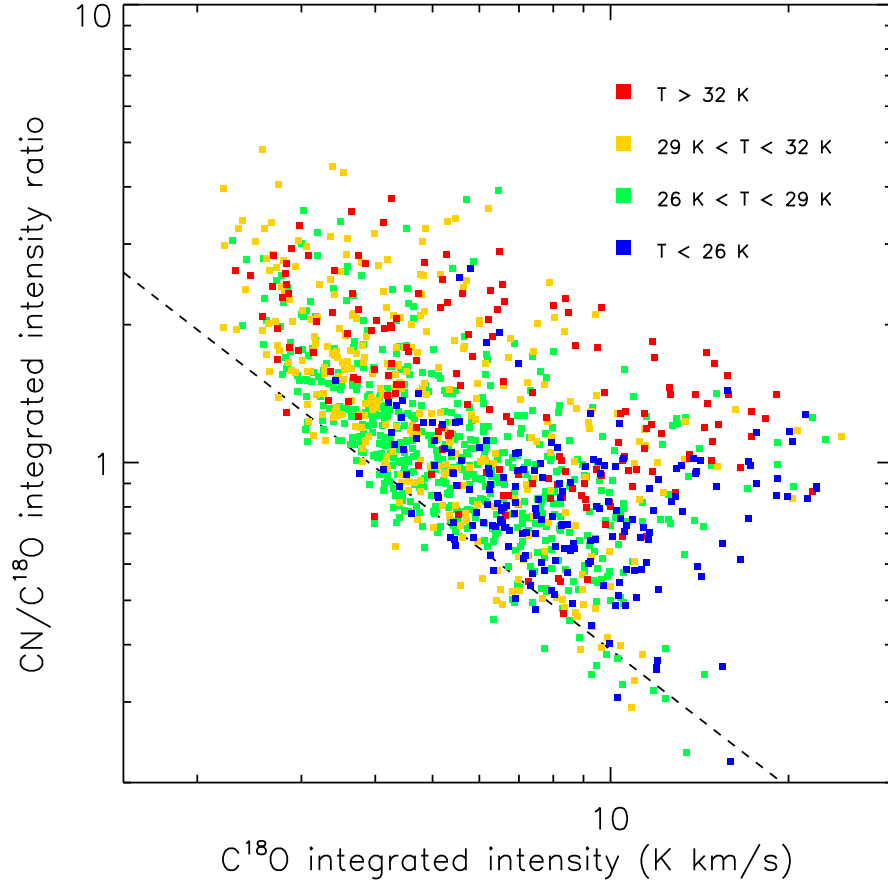


Fig. 6.— CN/C¹⁸O integrated intensity ratios plotted against C¹⁸O integrated intensities for regions where CN/C¹⁸O ratios are detected with S/N>3. The data are color-coded into four levels according to the dust temperature. The dashed line indicates the typical 3 σ detection limit of CN.

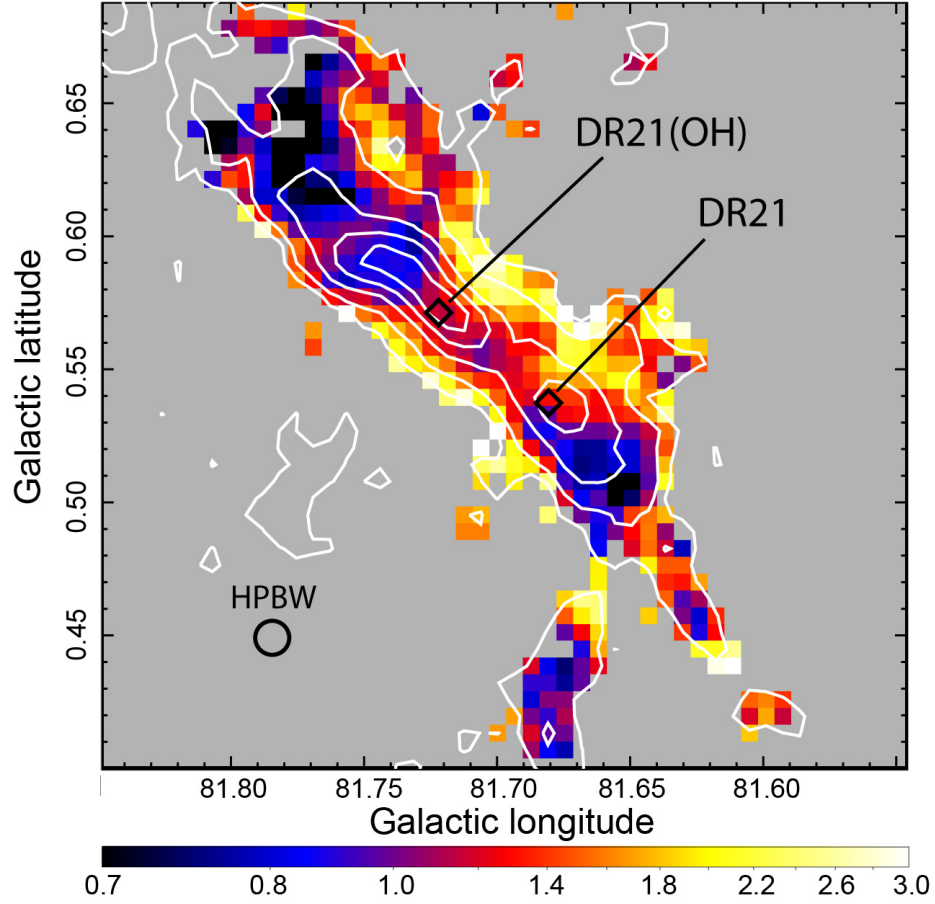


Fig. 7.— CN/C¹⁸O integrated intensity ratio map of DR21. Contours indicate C¹⁸O integrated intensity at 2.5, 5, 10, 15, 20 K km s⁻¹. Diamonds indicate positions of the star-forming sites, DR21 and DR21(OH).